


# Intranuclear inclusions in hepatocellular carcinoma contain autophagy-associated proteins and correlate with prolonged survival

Suzan Schwertheim<sup>1</sup> , Daniela Westerwick<sup>1</sup>, Holger Jastrow<sup>2</sup>, Sarah Theurer<sup>1</sup>, Christoph M Schaefer<sup>1</sup>, Julia Kälsch<sup>1,3</sup>, Dorothe Möllmann<sup>1</sup>, Martin Schlattjan<sup>1</sup>, Heiner Wedemeyer<sup>3</sup>, Kurt Werner Schmid<sup>1,4</sup> and Hideo A Baba<sup>1\*</sup>

<sup>1</sup>Institute of Pathology, University Hospital of Essen, University of Duisburg-Essen, Essen, Germany

<sup>2</sup>Institute of Anatomy, University Hospital of Essen, University of Duisburg-Essen, Essen, Germany

<sup>3</sup>Department of Gastroenterology and Hepatology, University Hospital of Essen, University of Duisburg-Essen, Essen, Germany

<sup>4</sup>West German Cancer Centre Essen (WTZE), University Hospital of Essen, University of Duisburg-Essen, Essen, Germany

\*Correspondence: Hideo A Baba, Institute of Pathology, University Hospital of Essen, University of Duisburg-Essen, Hufelandstrasse 55, 45147 Essen, Germany. E-mail: hideo.baba@uk-essen.de

## Abstract

For decades, intranuclear inclusions in many normal and neoplastic cells have been considered to be mere invaginations of cytoplasm into the nucleus without any notable function or influence on disease. We investigated such inclusions in 75 specimens of hepatocellular carcinoma (HCC). In this context we demonstrate that these inclusions are true inclusions, completely closed and delimited by the nuclear membrane, containing degenerate cell organelles and lysosomal proteins. Moreover, their occurrence was positively associated with patient survival but not with tumour grade or stage. In a standardised area a mean of 124 inclusions per specimen was present in the tumorous liver tissue in contrast to 5 inclusions in the non-tumorous adjacent section and 89% of all scrutinised HCC showed at least one membrane-bound nuclear inclusion. Ultrastructural characterisation by transmission electron microscopy revealed degenerative materials such as residues of lysosomes, endoplasmic reticulum and Golgi apparatus within the inclusions. Due to the fact that the content of the inclusions appears to be more condensed than cytoplasm and contains fewer intact cell organelles, we assume that they are not mere invaginations of cytoplasm. Three dimensional (3D) reconstruction of isolated and immunofluorescence stained nuclei showed that the inclusions are completely located within the nucleus without any connection to the cytoplasm. The limiting membrane of the inclusions contained lamin B suggesting nuclear membrane origin. The content of the inclusions stained for the autophagy-associated proteins p62, ubiquitin, LC3B, cathepsin B and cathepsin D. Triple immunofluorescence staining followed by 3D reconstruction revealed co-localisation of p62, ubiquitin and LC3B in the same inclusion. Our observations uncover that these inclusions are real inclusions completely surrounded by the nucleus. We propose that the presence of autophagy-associated proteins and proteases within the inclusions contribute to beneficial survival.

**Keywords:** intranuclear inclusions; autophagy; lysosomal proteins; HCC

Received 29 October 2018; Revised 5 February 2019; Accepted 28 February 2019

No conflicts of interest were declared.

## Introduction

Cell inclusions have been known for a long time. In 1883 the later Nobel laureate Paul Ehrlich described inclusions in the protoplasm of cells in diabetic patients, which he designated as vacuoles [1]. In the 1940s Schiller *et al* investigated nuclear inclusions in

hepatocytes and noted that their occurrence in the liver was associated with certain cell criteria, such as enlarged nuclei [2,3]. Until that time, all investigations and observations were limited to the mere description of morphological aspects of nuclear inclusions in light microscopy. During the next decade *in vivo* models showed that externally administered substances were

able to induce the development of nuclear inclusions. Long-term colchicine application induced nuclear inclusions in mouse hepatocytes, whereas discontinuation of colchicine resulted in their regression [4]. With the introduction of electron microscopy ultrastructural details of the nuclear inclusions have been analysed. It was possible to identify nuclear inclusions with or without a limiting membrane. The limiting membrane showed a similar morphology to the nuclear membrane [5]. The entrapped content within the inclusions contained cytoplasmic structures, often with degenerative changes, suggesting that the nuclear inclusion is completely separated from the cytoplasm [6].

Nuclear inclusions can also be found in humans. Basically, two morphologically distinct types of nuclear inclusions can be distinguished. Inclusions attributed to accumulation of viral particles or glycogen, which are not membrane bound, and inclusions which are delimited by the nuclear membrane [7]. Nuclear inclusions are found in 75% of patients suffering from non-alcoholic steatohepatitis (NASH) but only in 10% of patients with alcoholic hepatitis [8]. However, the authors of this paper did not differentiate between inclusions with or without limiting membrane. In hepatocellular carcinoma (HCC) nuclear inclusions with a sharply demarcated circular border are a regular finding. A study on fine needle aspirations of 320 HCCs showed nuclear inclusions with cytoplasmic content in 73% of the cases, whereas they were present in only 7% of non-neoplastic specimens [9].

Nuclear inclusions are not limited to hepatocytes but are also found in neural tissue. Meningiomas showed intranuclear inclusions, which display contents similar to autophagic vacuoles with lysosomal bodies suggesting an active macroautophagy process [10].

Other studies found some pigmented neural cells, so called Marinesco bodies, which are spherical eosinophilic intranuclear inclusions, in the substantia nigra and locus ceruleus [11]. These inclusions were immunohistochemically positive for proteins involved in proteosomal degradation and autophagy [12] suggesting that these inclusions serve as a place for protein degradation. In an earlier study using transgenic mice with deletion of survivin in hepatocytes [13] we detected numerous nuclear inclusions containing proteins of the chromosomal passenger complex (CPC); these proteins are partners of survivin. While in wild type mice the proteins of the CPC are located at the centromere region of chromosomes, in survivin KO mice these proteins were no longer detectable at the centromeres but, strikingly, instead in nuclear inclusions [13]. It is not known why the lack

of survivin causes mislocalisation of the CPC proteins in nuclear inclusions but it can be supposed that these proteins may be degraded in the inclusions. To clarify if autophagy-associated proteins [14] are detectable in these nuclear inclusions we looked for the presence of the proteins p62/sequestosome1, ubiquitin, LC3B, cathepsin B and cathepsin D by immunohistochemistry. Notably, p62 is also involved in several biological processes [15,16] including NF $\kappa$ B activity, cell proliferation [17,18], apoptosis [19], Keap1-Nrf2 system [20], DNA repair [21,22] and is associated with several cancer types [23–31]. In this study we investigated the occurrence of nuclear inclusions in hepatocytes of patients with HCC, characterised the inclusions by means of electron microscopy and immunohistochemistry, and explored if these inclusions have any impact on patient survival.

## Material and methods

### Patients

This study comprised 75 patients with histologically proven HCC. The tumours were diagnosed between 1999 and 2005 and were retrieved from the files of the Institute of Pathology, University Hospital of Essen, Germany. In all cases uniformly processed formalin-fixed and paraffin-embedded (FFPE) material from untreated patients was available. Slides were prepared and stained with H&E according to institutional standards. The tumours were diagnosed according to the current WHO criteria [32] and classified according to the TNM-system (8th edition). Patient and tumour characteristics are shown in Table 1.

Detailed and complete clinical records and follow-up data were available in 73 cases. Thirty-two patients in this study died during the observation period (day 55–3009 post surgery). Eighteen patients developed tumour recurrence during the observation period or during their lifetime. The range of recurrence-free survival of the patients was 55–2910 days after the initial treatment.

Informed consent was obtained from every patient. The study was in accordance with the Helsinki Declaration of 1975 and approved by the Ethics Committee (Institutional Review Board) of the University Hospital Essen (reference number: 16-6917-BO).

### Tissue microarray construction and immunohistochemistry

The expression of selected candidate proteins was investigated by immunohistochemistry using tissue

Table 1. Clinical and pathological parameters of the study group

	All (n = 75)
Mean age (years) at diagnosis (range)	62 (17–99)
Gender (male/female)	56/19
Liver morphology	
Non-cirrhosis	44
Cirrhosis	25
Fibrosis	6
Background	
Underlying disease unknown	43
Alcohol abuse	2
Hepatitis B	13
Hepatitis C	16
Hepatitis B + C	0
Alpha-1-antitrypsin deficiency	1
Primary biliary cirrhosis	0
Autoimmunhepatitis	0
Tumour staging	
pT1a/b	37
pT2	25
pT3	8
pT4	5
Grading	
G1	9
G2	41
G3/G4	25
Nodal status	
pN0	71
pN1	4
Lymph vessel infiltration	
L0	75
Blood vessel infiltration	
V0	42
V1	33
Resection status	
R0	63
R1	10
R2	2
Observation period (in days) post surgery	
Minimum	55
Maximum	3009

microarrays (TMAs). Tumour areas were selected with matched H&E stained slides and marked on the donor block. In case of tumour heterogeneity, areas with lowest degree of differentiation were selected. The TMAs were constructed using a manual tissue-array instrument (Beecher Instruments, Silver Spring, MD, USA). Three 1-mm-thick tissue cores were taken from each liver carcinoma specimen. Each TMA contained three corresponding tumour-free liver tissue cores as controls and cores with myocardial tissue for TMA orientation. Additionally, one section from each TMA was stained with H&E.

Ten sections (3–5 µm) were cut from each TMA; the paraffin sections were dewaxed and pre-treated. Immunostaining for ubiquitin, p62, LC3B, cathepsin B and cathepsin D was carried out on an automated

staining device (Dako Autostainer, Dako, Glostrup, Denmark). Detailed information on antibodies used and staining protocols are given in the supplementary material, Table S1. For negative controls (included in every run), slides were incubated with non-immune immunoglobulin at the same concentrations as the primary antibody instead of the primary antibody. One observer (DW) evaluated the H&E stained slides and the immunohistochemical stains. To compensate for tumour heterogeneity, membrane-bound intranuclear inclusions were counted in all ten serial sections from each case; only cases with evaluable material on all ten serial sections were included. The number of inclusions was counted in a standardised area, calculated by:  $10 \times (3 \times 1 \text{ mm tissue cores}) = 10 \times (3 \times 0.78 \text{ mm}^2) = 23.5 \text{ mm}^2$ . The qualitative detection of membrane-bound nuclear inclusions was recorded as positive (1) or negative (0). Cases containing at least one membrane-bound nuclear inclusion were considered positive. The enumeration of the inclusions on the immunohistochemical sections was enabled by the haematoxylin counterstain. Additionally, we examined the immunostains within the nuclear inclusions. Due to the small size of the nuclear inclusions and staining surface, the staining intensity was not quantified. Cases with positively stained membrane-bound nuclear inclusions were classified as positive (1) or negative (0).

### Transmission electron microscopy

For transmission electron microscopy (TEM), fresh tissue from liver biopsy of a representative HCC patient was fixed in 2% glutaraldehyde in 0.1 M cacodylate buffer (cb), pH 7.3, for 4 h at room temperature, washed in cb, post-fixed with 1% osmium tetroxide in cb, dehydrated in a graded series of alcohol and embedded in epoxy resin. To define blocks of adequate quality semi-thin sections were stained with basic fuchsin and methylene blue. Ultrathin sections from selected blocks were mounted on copper grids, double-stained with uranyl acetate (1%) and lead citrate (0.4%) and examined using a Zeiss TEM 902A (Zeiss, Oberkochen, Germany). Digital image acquisition was performed with help of an attached Morada slow-scan-CCD camera and the ITEM 5.2 software (both Olympus Soft-imaging-Systems, Münster, Germany).

### Three dimensional imaging of double immunofluorescence-labelled isolated nuclei

We performed three dimensional (3D) imaging on isolated complete nuclei to visualise the location of the

inclusion within the nucleus. Upon scanning the whole nucleus the spatial position of the inclusion in relation to the nucleus can be studied. For double immunofluorescence tumour cell nuclei of a representative HCC patient were isolated. Paraffin sections (60 µm thick) were placed in a 1.5 ml reaction tube, deparaffinised in xylene and centrifuged. The pellet was rehydrated in 100, 90 and 70% ethanol; disrupted by a homogeniser, centrifuged and pre-treated with EDTA buffer (pH 9.0) for 60 min at 99.5 °C. For immunostaining cells were permeabilised in a 1.5 ml reaction tube with 0.5% saponin and 2% BSA for 60 min at RT and then incubated with the primary antibodies lamin B (Santa Cruz Biotechnology, Santa Cruz, CA, USA) and p62 (Enzo Life Sciences, Farmingdale, NY, USA) overnight at 4 °C. Cells were centrifuged, washed and incubated with the secondary antibodies DyLight<sup>®</sup> 488-conjugated donkey anti-goat IgG (Abcam, Cambridge, UK) and Alexa Fluor 594-conjugated chicken anti-rabbit (Life Technologies, Grand Island, NY, USA). Anti-lamin B antibody was labelled with DyLight<sup>®</sup> 488 and anti-p62 antibody with Alexa Fluor 594; both were diluted 1:100 and incubated for 2 h at 37 °C (see supplementary material, Table S2). After nuclear staining with DAPI (Sigma-Aldrich, Steinheim, Germany), cells were mounted in anti-bleeding medium (Vectashield; Vector Laboratories Inc., Burlingame, CA, USA). Images were obtained using a Leica TCS SP8 STED confocal microscope (Leica Microsystems, Buffalo Grove, Illinois, USA) and were analysed with the Application Suite X software (Leica Microsystems). 3D reconstruction based on sectional images was performed using the open source software Fiji (ImageJ; [www.fiji.sc](http://www.fiji.sc)) and z-stacks were deconvolved using Huygens Professional software (Scientific Volume Imaging; [www.svi.nl/ContactSVI](http://www.svi.nl/ContactSVI)).

#### Triple immunofluorescence and 3D reconstruction of tissue sections

Spatial localisation of p62, ubiquitin and LC3B was investigated by triple immunofluorescence staining and subsequent 3D reconstruction. One-µm-thick FFPE tissue sections (HCC) were cut, dewaxed, rehydrated and pre-treated with Target Retrieval Solution (Agilent Technologies, Ratingen, Germany) at pH 9.0 for 20 min at 97 °C. For triple labelling immunofluorescence the primary antibodies anti-p62 (MBL, Nagoya, Japan), anti-ubiquitin (Santa Cruz Biotechnology) and anti-LC3B (Nano Tools, Hamburg, Germany) were used. The secondary antibodies used were Cy5-conjugated donkey anti-rabbit IgG (Dianova, Hamburg, Germany), DyLight<sup>®</sup> 488-conjugated donkey anti-goat IgG (Abcam) and

Alexa Fluor 555-conjugated donkey anti-mouse IgG (Thermo Fisher Scientific, Waltham, MA, USA). Anti-p62 antibody was labelled with Cy5, anti-ubiquitin antibody with DyLight<sup>®</sup> 488 and anti-LC3B antibody with Alexa Fluor 555; all were diluted 1:100 and were incubated for 1 h at RT (see supplementary material, Table S3). DNA was stained with DAPI; image analysis and 3D reconstruction were performed as described above.

#### Statistical analysis

Statistical analysis was performed using the Statistical Package for Social Sciences (SPSS 24.0, Chicago, IL, USA). Relationships between categorical parameters were investigated using two-sided Fisher's exact test. Additionally, we performed survival analysis to study whether the sole presence of membrane-bound nuclear inclusions were related to patient survival. Overall survival (OS) curves were estimated using the Kaplan–Meier method, and differences in survival curves were compared by the log-rank test;  $p \leq 0.05$  was defined as statistically significant.

## Results

#### Occurrence of nuclear inclusions in HCC and in non-neoplastic liver

Analysis of 10 TMA sections in the 75 HCC cases showed evaluable material in 70 tumour tissue sections (TTS) and in 59 adjacent normal tissue sections (NTS) on all serial sections. The number of membrane-bound intranuclear inclusions varied between 0 and 1369/23.5 mm<sup>2</sup> in the TTS and between 0 and 50/23.5 mm<sup>2</sup> in the NTS per case (Table 2). These nuclear inclusions had different shapes, numbers and sizes (Figure 1A,B). Also, the content of the membrane-bound nuclear inclusions was often heterogeneous with uneven H&E staining. The staining reaction was often similar to that of the cytoplasm but quite different from that of the karyoplasm (Figure 1A,B). There was no obvious difference between the intranuclear inclusions in the TTS (Figure 1A) and in the adjacent NTS (Figure 1B).

#### Ultrastructural characterisation of nuclear inclusions

To examine the intranuclear inclusions in HCC more in detail, we performed TEM. We observed that these inclusions are filled with degenerative material such as

**Table 2.** Quantitative parameters of the intranuclear inclusions in the HCC cohort

	Tumour tissue	Adjacent normal tissue
Number of valid cases	<i>n</i> = 70	<i>n</i> = 59
Number of valid cases with the presence of at least 1 intranuclear inclusion	<i>n</i> = 62	<i>n</i> = 48
Mean count of intranuclear inclusions/case (range)*	124 (0–1369)	5.36 (0–50)

\*Inclusions were counted in a standardised area of 23.5 mm<sup>2</sup> (ten serial sections of each case). The values presented are the mean of valid cases with evaluable material on all ten serial sections.

remnants of Golgi apparatus, endoplasmic reticulum and of lysosomes (Figure 2A,B). Comparing cytoplasm and the plasma in the nuclear inclusion, both show similarities but also differences: First, the plasma of the nuclear inclusion appears to be more condensed than the cytoplasm. Second, they differ regarding their contents. Within the intranuclear inclusions there are fewer intact cell organelles (Figure 2A,B). We observed membrane-limited inclusions lacking contact to the outer membrane of the nucleus or to the cytoplasm (Figure 2A, Ai). This indicates that these degradation processes take place completely inside the intranuclear inclusions. The inclusions are lined by the two (inner and outer) nuclear membranes with attached membrane-associated heterochromatin (h). We detected several nuclei with invaginations of surrounding cytoplasm (Figure 2B, Bi). This supports our suggestion that intranuclear inclusions develop by later closure of the invagination (see 3D reconstructions below). Similar results are demonstrated in Figure 2C,D.

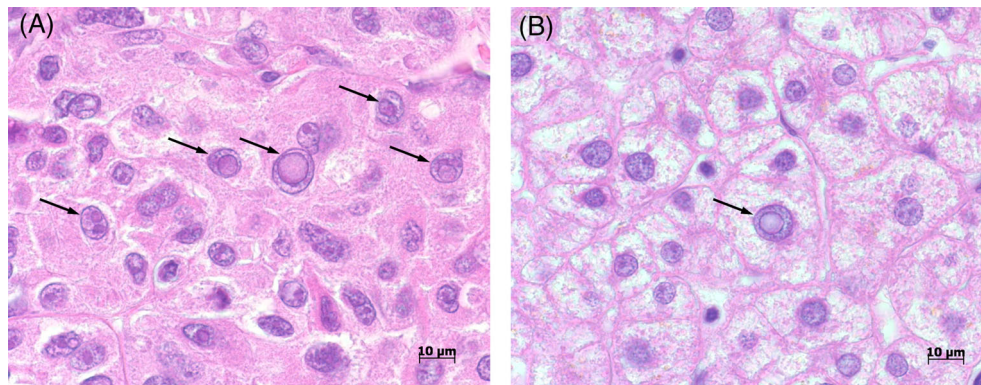


**Figure 1.** Intranuclear inclusions in HCC and in non-neoplastic liver. The image depicts the intranuclear inclusions in a representative patient from the HCC cohort in the TTS (A) and in the adjacent NTS (B). Their number per nucleus varies from one to three or more inclusions (arrows). The nuclei of cells with membrane-bound nuclear inclusions (arrows) are often large compared to cells without nuclear inclusions and the karyoplasm is bright with loosely distributed chromatin (H&E stain, original magnification  $\times 1000$ ).

Inclusions are completely surrounded by the nucleus

To analyse whether these membrane-bound nuclear inclusions, are merely nuclear membrane invaginations with persistent cytoplasmic contact or ‘real’, exclusively intranuclear, compartments completely separated from the cytoplasm, we performed 3D nuclear imaging with double immunofluorescence (lamin B and p62). We found no connection between the content of the nuclear inclusion and the cytoplasm in the studied section planes. We detected strong positive p62 immunostaining in the nucleoplasm and weak to moderate immunoreactivity in the limiting membrane of the nuclear inclusion. The limiting membrane of the inclusion was positive for lamin B which points to an origin from the nuclear membrane (Figure 3A–D; see supplementary material, Movie S1). We investigated additionally the tumour cell nuclei of three HCC patients by 3D nuclear imaging with lamin B immunofluorescence. 3D reconstructions of at least two nuclei with inclusions per patient also showed the location of the inclusion within the nucleus (see supplementary material, Figure S1).

#### Autophagy associated proteins in nuclear inclusions

We performed immunohistochemistry studies to investigate whether there is a connection between the occurrence of intranuclear inclusions and autophagy. Ubiquitin, p62, LC3B, cathepsin B, and cathepsin D immunohistochemistry was available for 71–74 TTS and 61–70 NTS cases while there was lack of suitable materials in the other cases.

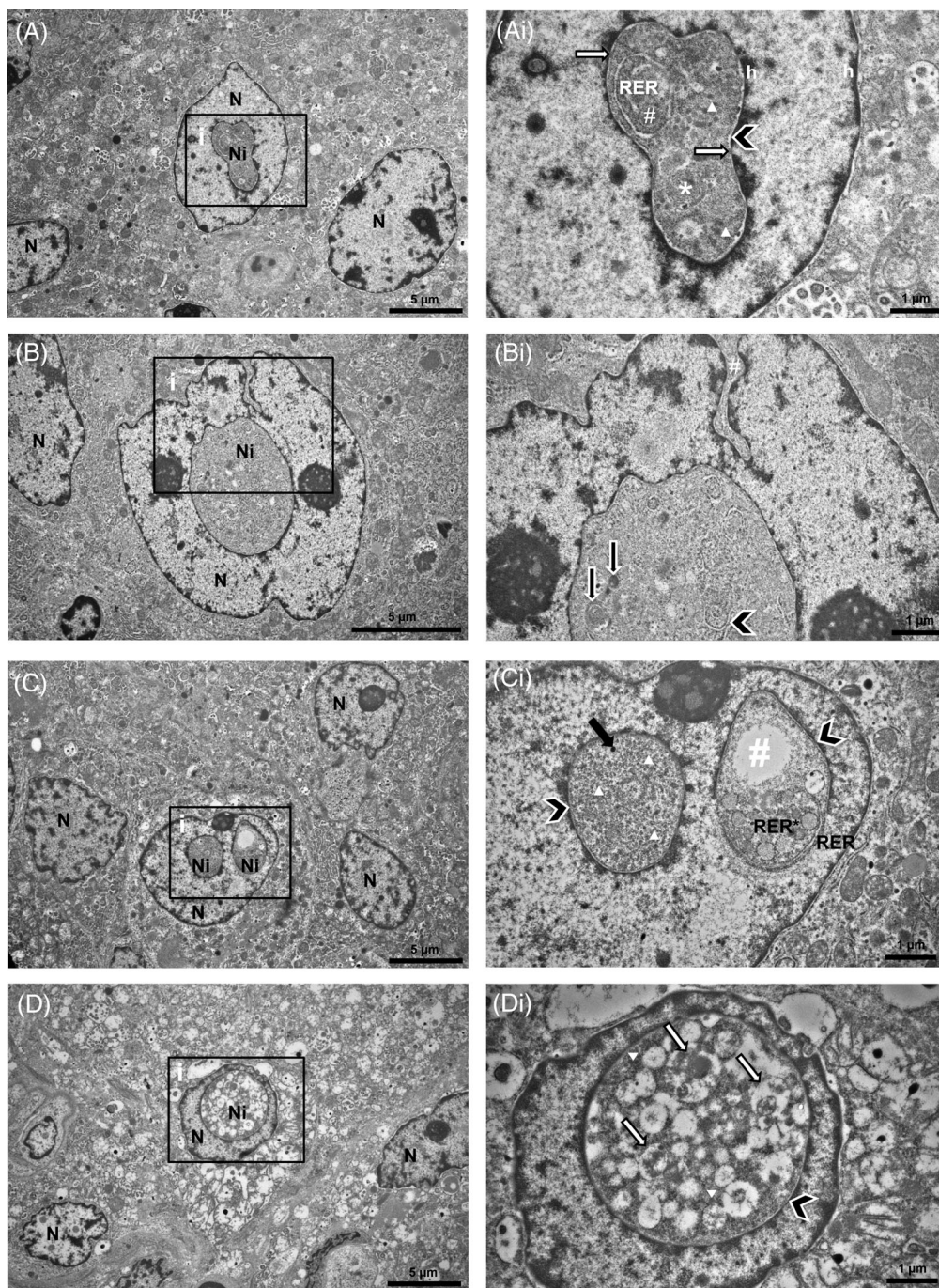


Figure 2. Legend on next page

We found positive immunoreactivity for all investigated proteins in the nuclear inclusions (Figure 4). Briefly, 38 of 74 (51.4%) TTS and 9 of 62 (14.5%) NTS showed at least one membrane-bounded nuclear inclusion with positive p62 immunostaining (Table 3 and Figure 4). For ubiquitin 23 of 71 (32.4%) TTS and 3 of 62 (4.8%) NTS showed at

least one membrane-bounded nuclear inclusion with positive immunostaining (Figure 4); for more details see Table 3. The immunohistochemical staining pattern of the intranuclear inclusions was similar in TTS and NTS, with cathepsin B staining most common in both, followed by p62 and cathepsin D (Table 3).

## Association of ubiquitin with p62, LC3B, cathepsin B and cathepsin D

Chi-square cross table analysis was used to investigate relationships between p62, ubiquitin, LC3B, cathepsin B and cathepsin D immunostaining reactivity in the intranuclear inclusions. Cases were classified as positive (1) if at least one membrane-bound inclusion showed positive immunostaining, whereas cases lacking stained inclusions were classified as negative (0). Analysis of the 23 TTS cases with positive ubiquitin immunostaining revealed that 22 of them also have nuclear inclusions with positive p62 immunostaining ( $p \leq 0.001$ ) and 10 showed LC3B immunoreactivity ( $p \leq 0.001$ ). Also, there was a significant relationship between ubiquitin and cathepsin B and cathepsin D immunoexpression in the intranuclear inclusions ( $p \leq 0.001$ ) in TTS. Analysis of the immunoreactivity in the intranuclear inclusions of NTS showed no significant association between ubiquitin and p62 immunostaining ( $p = 0.053$ ; Table 4).

We observed a significant association between the expression of p62 and LC3B ( $p \leq 0.001$ ) in TTS as 13 of the 14 cases with LC3B – stained nuclear inclusions were also positive for p62.

A total of 25 of the 28 cases showing positive cathepsin D immunostaining in the membrane-bound nuclear inclusions revealed an additional immunoreactivity for cathepsin B ( $p \leq 0.001$ ). We found no significant associations regarding immunoreactivity in the intranuclear inclusions of NTS.

## Spatial co-localisation of proteins in nuclear inclusions

To investigate if these autophagy-associated proteins are located within the same inclusion, we performed

triple immunofluorescence labelling followed by STED microscopy and 3D reconstruction of serial sections. Figure 5 depicts a DAPI-stained nucleus with intranuclear inclusions. Analysis of this image on several planes revealed the co-localisation of ubiquitin, p62 and LC3B in the same inclusion proven by the formation of the merged colour white (Figure 5, circle). Additionally, we detected ubiquitin, p62 and LC3B-stained Mallory–Denk bodies in the cytoplasm (Figure 5, square); their immunoreactivity for ubiquitin, p62 and LC3B and association with autophagy is well documented [33].

## Prognostic relevance of nuclear inclusions in HCC patients

### Statistical analysis of associations between the presence of inclusions and underlying diseases

Regarding underlying diseases, our study did not detect a significant relationship between the occurrence of inclusions and gender, tumour grading, staging, underlying viral infections or aetiological factors of non-virally induced cirrhosis in the tumour tissue and in the adjacent NTS (Table 5).

### Correlation of the presence of intranuclear inclusions with survival

To check if disease-specific OS depends on the occurrence of membrane-bound nuclear inclusions, we used Kaplan–Meier survival curves (Figure 6).

The study was based on ten serial sections from each TMA. Information on OS was available for 68 of the 70 valid HCC cases. Sixty of these 68 patients had at least one membrane-bound intranuclear inclusion. Most, 39 (65%), of these 60 patients survived but 7 (87.5%) of 8 patients who had no intranuclear

**Figure 2.** Transmission electron microscopic (TEM) images of intranuclear inclusions in HCC. (A) In the centre of the image is a nucleus (N) with one large inclusion (Ni) whose boundary corresponds to the nuclear membrane. This inclusion is lined by the two (inner and outer) nuclear membranes with attached membrane-associated heterochromatin (h) (A, Ai); increased magnification (Ai) depicts the typical double membrane (arrowhead) with a few nuclear pores (arrows). The intranuclear inclusion is bordered just by the nuclear membrane with no contact and a distance of over 1  $\mu\text{m}$  to the outer membrane of the nucleus. The content of the nuclear inclusion appears to contain more electron dense material than the cytoplasm. Increased magnification (Ai) reveals a well preserved ring of rough endoplasmic reticulum (RER) close to a possible lysosome (#). Possible remnants of a Golgi apparatus (asterisk) and small vesicles of homogeneous high electron-density resembling lysosomes (triangles) are also seen. Image (B) shows a large nucleus with a nuclear inclusion (Ni). A deep but thin invagination of cytoplasm into the nucleus oriented towards the inclusion is present (#; Bi). Parts of the RER (arrowhead) and heterolysosomes (arrows) are seen within the nuclear inclusion. Image (C) depicts four hepatocyte nuclei (N) one of which has two prominent Ni, which are shown enlarged on the right (Ci). Both inclusions are bordered by a nuclear membrane (arrowhead). While the left inclusion has abundant finer granular material resembling ribosomes (triangles) and only one small lysosome (solid black arrow), the right one has a large vacuole # with homogeneous content suggesting lipid and, below, usual RER (RER) is present as in the cytoplasm, and is rather dilated RER (RER\*). (D) Degenerating hepatocyte with an enormous nuclear membrane (arrowhead)-bordered inclusion (>5  $\mu\text{m}$  in diameter) detailed in image Di with plenty of partly confluent heterolysosomes (white arrows) embedded in electron-dense granular material possibly rich in ribosomes (triangles).

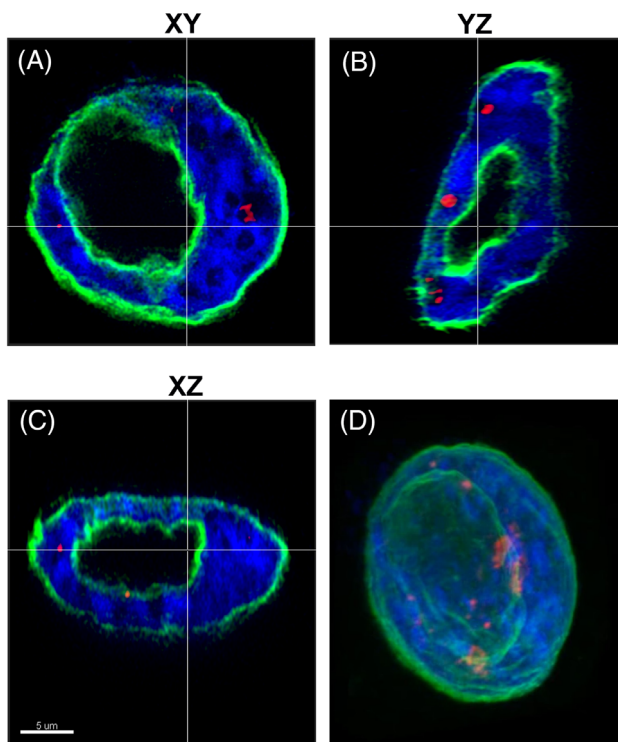


**Figure 3.** 3D imaging of double immunofluorescence-labelled (lamin B and p62) isolated cell nucleus in X-, Y- and Z-axes. A total of 272 optical sections of 0.1  $\mu\text{m}$  were imaged and used for 3D reconstruction. The representative image depicts a tumour cell nucleus with lamin B (green) stained nuclear membrane. Depending on the section plane, the nuclear shape varies from round to slightly irregular, showing one nuclear inclusion (A–C) with marginal lamin B positivity. At least one narrow karyoplasmic space is found in all sectional planes, separating the membrane of the nuclear inclusion from the actual nuclear membrane. There is no DAPI (blue) staining within the nuclear inclusion; p62 (red) immunoreactivity in the nucleus and in the limiting membrane of the nuclear inclusion is shown. Additionally a section of the movie “3D nuclear imaging with double immunofluorescence” (see supplementary material, Movie S1) is shown (D).

inclusions died during the observation period. Kaplan–Meier survival analysis showed a significant survival benefit for patients with membrane-bound intranuclear inclusions in HCC ( $p = 0.020$ ; Figure 6).

## Discussion

Nuclear inclusions were first described in light microscopy more than 100 years ago [1–3]. Since then they have been detected in many normal and neoplastic tissues [6–8]. Little is known about the origin or the

function of these peculiar nuclear changes that most clinical pathologists see in their daily routine work. So far it is believed that the occurrence of nuclear inclusions is a rather non-specific morphological feature. The aim of the study was to characterise the membrane bound nuclear inclusions in HCCs in respect of origin, content and possible function.

In our cohort, 89% of HCC showed at least one membrane bound nuclear inclusion with a mean of 124 inclusions/23.5  $\text{mm}^2$  per specimen in contrast to 5/23.5  $\text{mm}^2$  inclusions in the adjacent non-neoplastic liver tissue. A previous study investigating patients with chronic hepatitis B also detected nuclear inclusions/vacuoles in hepatocytes but no differentiation between inclusions with or without limiting membrane was made [34].

A transgenic mouse model of hepatitis B surface antigen mediated hepatitis exhibited nuclear inclusions in murine hepatocytes and the presence of inclusions correlated with oxidative stress and proliferation [35]. The authors did not investigate the inclusions by means of electron microscopy to show a limiting nuclear membrane. Furthermore, no nuclear invagination containing cytoplasm was depicted.

It is debated whether nuclear inclusions are true inclusions or only nuclear invaginations of the cytoplasm due to irregular nuclear shape. In 2010, a review article differentiated between nuclear inclusions and pseudoinclusions. While nuclear inclusions are not membrane bound and present foreign material such as viral substances, pseudoinclusions are membrane bound and develop by herniation of the cytoplasm into the nucleus [7]. In contrast, we were able to detect at least some inclusions which are completely surrounded by the nucleoplasm. It is very likely that these inclusions developed by invagination of the cytoplasm into the nucleus delimited by the double layered nuclear membrane followed by later closure of the invagination. The 3D reconstruction of the intranuclear inclusions in this study supports this mechanism (Figures 3 and 5).

We demonstrate that these intranuclear inclusions are true inclusions, completely closed and not mere invaginations of cytoplasm into the nucleus. First, this is supported by our TEM pictures showing nuclei with nuclear inclusions and invaginations, both of which are limited by a nuclear membrane. The content of the inclusions is more condensed than cytoplasm and contains fewer intact cell organelles suggesting that the nuclear inclusions are not a simple invagination of the cytoplasm into the nucleus (Figure 2). Second, the positive immunostaining for p62, ubiquitin and LC3B was located almost exclusively in the nuclear



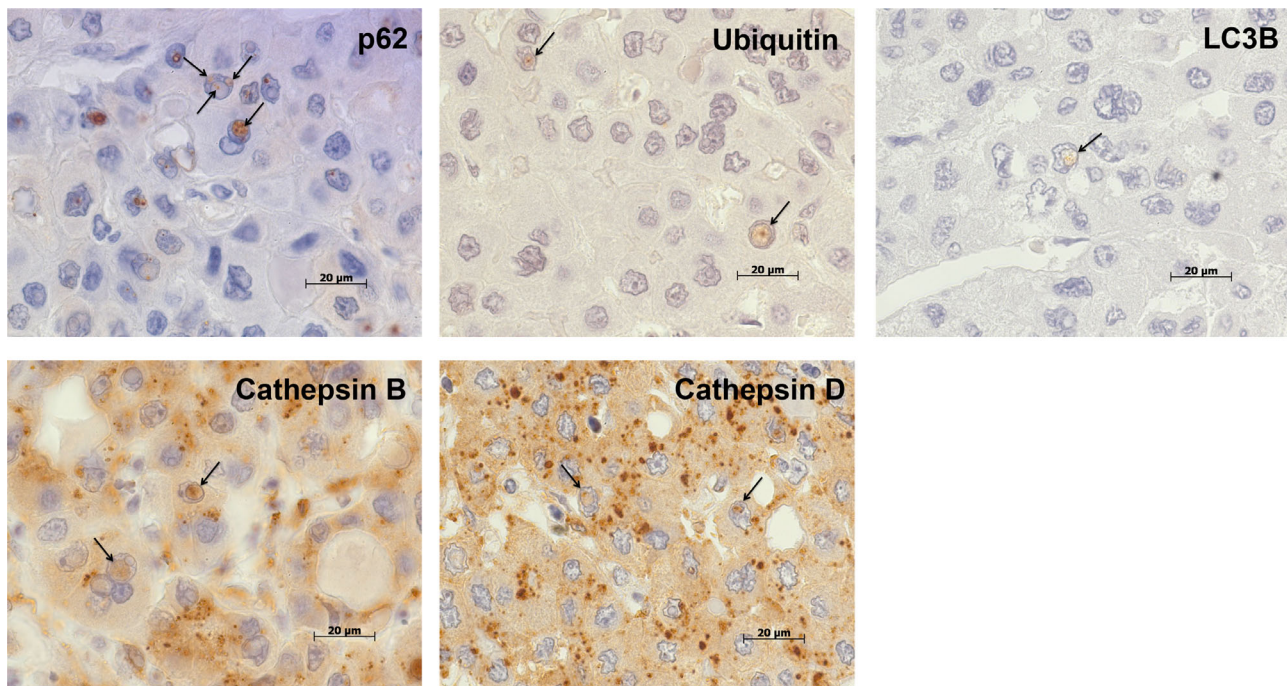


**Figure 4.** Immunoreactivity of autophagy-associated proteins in nuclear inclusions of HCC. p62 positive immunostaining is located almost exclusively within the membrane-bound nuclear inclusions; additionally the image depicts a nucleus with several intranuclear inclusions all showing positive p62 immunoreactivity. Strong ubiquitin staining is found exclusively in the nuclear inclusions and not in the cytoplasm. Nuclear inclusions also show positive staining for LC3B. For cathepsin B and cathepsin D, cytoplasmic staining is observed which has a similar staining intensity to the intranuclear inclusions. Arrows depict marked nuclear inclusions. Original magnifications:  $\times 1000$ .

**Table 3.** Number of cases with positive immunoreactivity in the intranuclear inclusions

Antibody	Tumour tissue	Adjacent normal tissue
	<i>n/n</i> valid cases (%)	<i>n/n</i> valid cases (%)
Cathepsin B	43/74 (58.1)	19/70 (27.1)
p62	38/74 (51.4)	9/62 (14.5)
Cathepsin D	28/72 (38.9)	7/61 (11.5)
Ubiquitin	23/71 (32.4)	3/62 (4.8)
LC3B	14/74 (18.9)	6/66 (9.1)

The number of cases containing at least one nuclear inclusion with positive immunoreactivity is depicted; *n* = number.

inclusions and not in the cytoplasm (Figure 4). In the case of an invagination of the cytoplasm into the nucleus, the cytoplasm should also be positively stained. Third, our studies of inclusions using immunohistochemistry (Figure 4) and electron microscopy (Figure 2) showed that these inclusions are completely closed in the 2D plane and 3D reconstruction clearly showed that the observed inclusion was completely located within the nucleus without any contact to the cytoplasm (Figure 3; see supplementary material, Movie S1). Already in the mid and late 1950s Kleinfeld *et al* [6] and Leduc *et al* [5] described

**Table 4.** Associations between p62, ubiquitin, LC3B, cathepsin B and cathepsin D immunoreactivity in the nuclear inclusions

Antibody	Tumour tissue		Adjacent normal tissue	
	<i>n</i>	<i>P</i> value	<i>n</i>	<i>P</i> value
Ubiquitin				
p62	22/71	< 0.001	2/62	0.053
LC3B	10/71	0.001	1/62	0.267
Cathepsin B	21/71	< 0.001	0/59	0.550
Cathepsin D	18/71	< 0.001	0/59	0.100
p62				
LC3B	13/74	0.001	2/62	0.206
Cathepsin B				
Cathepsin D	25/72	< 0.001	3/58	0.407

*n* = number of IHC positive nuclear inclusions/valid cases. *P* values were calculated using two-sided Fisher's exact test.

intranuclear inclusions with highly degenerate cytoplasmic components. They speculated that the inclusion content degenerates faster due to complete separation from the cytoplasm.

In this study we found within the nuclear inclusions cathepsin B and cathepsin D (Figure 4) which are proteases typically located in lysosomes. It is possible that these proteases digest the content of the inclusions and

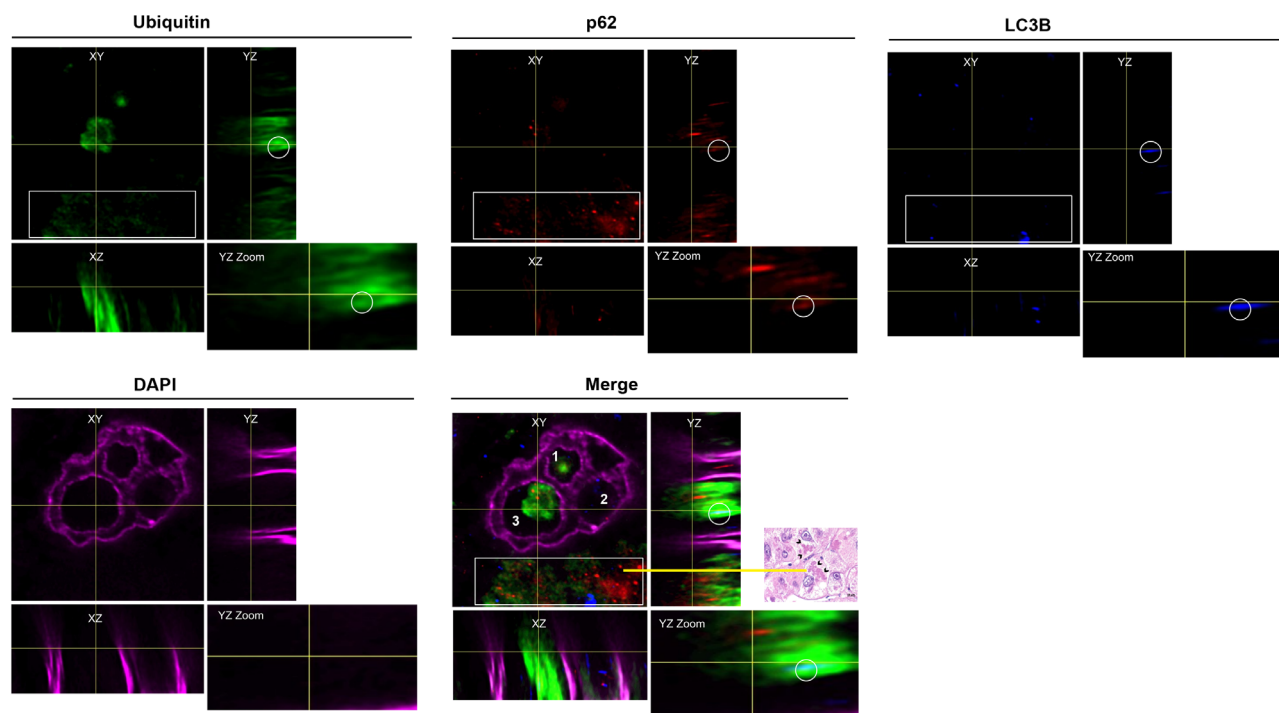


**Figure 5.** 3D reconstruction of triple immunofluorescence-labelled (ubiquitin, p62 and LC3B) HCC sections. 100 optical sections of 0.12  $\mu\text{m}$  were imaged and used for 3D reconstruction; a representative image is shown. DAPI staining (pink) shows the nucleus with intranuclear inclusions. Inclusion 1 (labelled in the merged image) contains strong ubiquitin staining (green) together with weaker LC3B (blue). In inclusion 2, the distribution of LC3B and p62 (red) is seen in the plane shown. Inclusion 3 shows in YZ planes strong ubiquitin staining together with strong p62 as well as LC3B immunoreactivity. Additionally, punctuated signals of endogenous LC3B indicating the induction of autophagy are seen. The merged colour white (circle) depicts the co-localisation of ubiquitin, p62 and LC3B in the same inclusion. Mallory–Denk bodies with positive immunoreactivity for ubiquitin, p62 and LC3B are present in the cytoplasm (rectangle); a representative H&E image shows Mallory–Denk bodies (arrowheads) in HCC.

contribute to the degeneration of the organelles. Some authors have already discussed the possibility of protein digestion in nuclear inclusions [10]. Meningiomas ultrastructurally showed nuclear inclusions with structures similar to autophagic vacuoles and lysosomal bodies suggesting an active macroautophagy process [10]. Pigmented neurons in the substantia nigra and locus ceruleus show nuclei with spherical eosinophilic inclusions known as Marinesco bodies. These inclusions contain ubiquitin, p62 and LC3 suggesting that Marinesco bodies are involved in autophagy [12]. We were able to find p62 positive inclusions in 51.4%, ubiquitin in 32.4% and LC3B in 18.9% of all nuclear inclusions. In addition, we found cathepsin B and D positive inclusions in 58.1 and 38.9%, respectively. This is in contrast to the Marinesco bodies which were negative for anti-lysosomal proteases [12].

We found a significant positive association of p62, ubiquitin, LC3B, cathepsin B and cathepsin D to each other. Such association however, does not mean that the proteins are present in the same inclusion. In order to

show a spatial association we used immunofluorescent triple staining and found p62, ubiquitin and LC3B in the same nuclear inclusion. In addition we found areas where all three proteins were co-localised. The presence of all three proteins in the same inclusion together with lysosomal proteins is highly suggestive for a proteolytic process similar to autophagy. This conclusion is provocative because autophagy is known to be active only in the cytoplasm. To prove the hypothesis of nuclear autophagy [36–41] additional functional experiments are necessary. However, we also observed positive immunoreactivity for the autophagy-related proteins (ATG)7, ATG12 and Beclin1 known to be involved in autophagosome formation [42], in the inclusions (see supplementary material, Figure S1 and Table S4). Duo *et al* pointed out the presence of several autophagy proteins including LC3, ATG5 and ATG7 in the nucleus [37]. Intriguingly, studies of Shin *et al* showed that co-activator-associated arginine methyltransferase 1 (CARM1)-dependent histone arginine methylation is a crucial nuclear event in autophagy [40]. Induction by

Table 5. Correlation of clinical parameters with the presence of intranuclear inclusions in the HCC cohort

	Tumour tissue	P value	Adjacent normal tissue	P value
Gender	<i>n</i> = 70		<i>n</i> = 59	
Male	47/54 (87%)	0.672	35/46 (76.1%)	0.100
Female	15/16 (93.8%)		13/13 (100%)	
Liver morphology	<i>n</i> = 70		<i>n</i> = 59	
Non-cirrhosis	36/43 (83.7%)	0.092	29/34 (85.3%)	0.433
Cirrhosis	21/21 (100%)		15/19 (78.9%)	
Fibrosis	5/6 (83.3%)		4/6 (66.7%)	
Background	<i>n</i> = 70		<i>n</i> = 59	
Non hepatitis	38/43 (88.4%)	1.000	32/36 (88.9%)	0.129
Hepatitis B + C	22/25 (88%)		14/21 (66.7%)	
Alcohol abuse	2/2 (100%)		2/2 (100%)	
Tumour staging	<i>n</i> = 70		<i>n</i> = 59	
pT1a/b	31/34 (91.2%)	0.053*	23/30 (76.7%)	0.274
pT2	23/24 (95.8%)		19/21 (90.5%)	
pT3	5/7 (71.4%)		3/5 (60%)	
pT4	3/5 (60%)		3/3 (100%)	
Grading	<i>n</i> = 70		<i>n</i> = 59	
G1	9/9 (100%)	0.660	5/7 (71.4%)	0.120
G2	34/40 (85%)		24/32 (75%)	
G3/G4	19/21 (90.5%)		19/20 (95%)	

P values were calculated using two-sided Fisher's exact test.

\*The relationship between the occurrence of inclusions and tumour staging is not significant but shows a trend ( $p = 0.053$ ) towards increased presence of inclusions in less progressive stages.

nuclear AMPK-SKP2-CARM1 signalling was also reported in HCC autophagy [41].

We detected p62 immunoreactivity in the intranuclear inclusions. p62 is a scaffold protein with

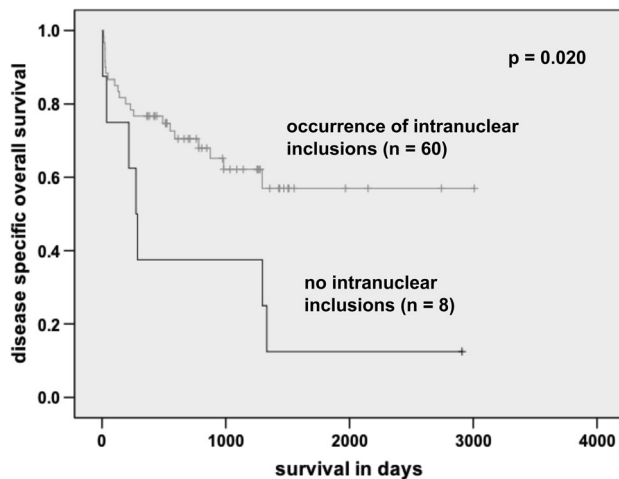


Figure 6. Kaplan-Meier survival curves in 68 valid HCC samples in relation to the presence of membrane-bound intranuclear inclusions. Patients who have no intranuclear inclusions in the tumour ( $n = 8$ ) exhibit a significantly decreased OS ( $p = 0.020$ ; log rank test). Disease specific OS was significantly associated with the occurrence of intranuclear inclusions. We counted the inclusions in a standardised area of 23.5 mm<sup>2</sup> (ten serial sections of each case). Only cases with evaluable material on all ten serial sections were included. Cases containing at least one membrane-bound nuclear inclusion were considered positive.

multiple domains that allows interaction with various binding partners and the regulation of several physiological processes in addition to the autophagy pathway [15–20,31]. High p62 can induce activation of Nrf2 or NF $\kappa$ B signalling pathways promoting cancer progression; nuclear p62 is involved in delivering ubiquitinated proteins for degradation [29,31]. Functional roles of nuclear p62 have been studied by Pankiv *et al* showing nucleocytoplasmic shuttling of p62 [43]. Our results regarding high p62 positivity in intranuclear inclusions might be due to several reasons including alterations in p62 nucleocytoplasmic shuttling.

Which process is responsible for alteration of the nuclear geometry inducing nuclear inclusions? It has been suggested that the cytoskeleton stabilises nuclear architecture by counterbalancing internal forces of the nuclear lamina and chromatin, and the nuclear architecture changes only when these stabilising factors are altered [44,45]. In an elegant study using *Drosophila* salivary gland cells, both weakening the nuclear envelope and forcing chromatin compaction resulted in distortions of the nuclear envelope and induced nucleoplasmic reticulum formation with similar morphology to nuclear inclusions [46]. The authors propose a model where inner nuclear envelop-chromatin tethers allow interphase chromosome movement to alter nuclear morphology [46].

Yet, the functional and clinical consequences are unknown. We found an interesting association of nuclear inclusions in HCC with OS showing that nuclear inclusions correlate significantly with increased

survival. Whether the occurrence of inclusions and patient survival is causal or only a correlation is not clear. To address this question, mechanistically driven experiments are necessary. However, it is interesting to speculate on how to explain the beneficial effect of nuclear inclusions on better survival. Assuming that the inclusions degrade proteins *via* lysosomal processes, (nuclear) oncogenes are perhaps targeted for degradation to eliminate their oncogenic effects. It has been shown in papillary thyroid carcinoma that beta-catenin is immunohistochemically detected in membrane bound nuclear inclusions [47]. Beta-catenin plays an important role in promotion of growth through activation of the Wnt pathway. We were also able to detect beta-catenin in HCC nuclear inclusions but found no association to beta-catenin mutation or survival (data not shown).

In summary, this study shows a high frequency of nuclear inclusions in HCC. Since at least some of the inclusions are completely enclosed by the nucleus, they should not be called pseudoinclusions but real inclusions. The presence of autophagy-associated proteins within the inclusions together with proteases like cathepsins suggests proteolytic properties associated with beneficial survival. These data suggest a highly dynamic nuclear geometry responding to biological processes throughout interphase which alters cellular behaviour.

### Acknowledgements

The authors thank Laura Malkus for technical assistance in the preparation of the samples for TEM. No funding was received specifically for this study.

### Author contributions statement

HAB, HW and KWS participated in the design of the study, made substantial contributions to the conception and aided in the data analysis. DW, HAB, JK, KWS and HW analysed immunohistochemical data and performed data collection and interpretation and revised the manuscript. HJ performed electron microscopy, drafted and discussed the data. HAB, KWS, DW, CS, JK, SS, ST, HJ, DM and MS performed data analysis, data interpretation, literature research and revised the article critically. CS, DM and MS conceived and carried out experiments. SS, CS, DM and MS generated figures. SS and DW performed statistical analysis. SS, HAB and DW wrote the manuscript, which had the approval of all the authors.

### References

- Ehrlich P. Ueber das Vorkommen von Glykogen im diabetischen und im normalen Organismus. *Z Klin Med* 1883; **6**: 33–46.
- Schiller E. Kerneinschlüsse und Amitose. *Z Zellforsch Mikrosk Anat* 1949; **34**: 356–361.
- Schiller E. Variationsstatistische untersuchungen ueber kerneinschlüsse und kristalle der menschlichen leber. *Z Zellforsch Mikrosk Anat* 1949; **34**: 337–355.
- Wessel W. Elektronenmikroskopische untersuchungen von intranuclearen Einschlusskoernern. *Virchows Arch Pathol Anat Physiol Klin Med* 1958; **331**: 314–328.
- Leduc EH, Wilson JW. An electron microscope study of intranuclear inclusions in mouse liver and hepatoma. *J Biophys Biochem Cytol* 1959; **6**: 427–430.
- Kleinfeld RG, Greider MH, Frajola WJ. Electron microscopy of intranuclear inclusions found in human and rat liver parenchymal cells. *J Biophys Biochem Cytol* 1956; **2**: 435–439.
- Ip Y-T, Dias Filho MA, Chan JKC. Nuclear inclusions and pseudoinclusions: friends or foes of the surgical pathologist? *Int J Surg Pathol* 2010; **18**: 465–481.
- Pinto HC, Baptista A, Camilo ME, *et al.* Nonalcoholic steatohepatitis. *Dig Dis Sci* 1996; **41**: 172–179.
- Soyuer I, Ekinci C, Kaya M, *et al.* Diagnosis of hepatocellular carcinoma by fine needle aspiration cytology. *Acta Cytol* 2003; **47**: 581–589.
- Jaskolski D, Papierz T, Liberski PP, *et al.* Ultrastructure of meningiomas: autophagy is involved in the pathogenesis of “intranuclear vacuoles”. *Folia Neuropathol* 2012; **50**: 187–193.
- Schochet SS Jr. Neuronal inclusions. In: *The Structure and Function of Nervous Tissue* Bourne GH (Ed). Academic Press: New York, 1972; 129–177.
- Odagiri S, Tanji K, Mori F, *et al.* Immunohistochemical analysis of Marinesco bodies, using antibodies against proteins implicated in the ubiquitin-proteasome system, autophagy and aggresome formation. *Neuropathology* 2012; **32**: 261–266.
- Hagemann S, Wohlschlaeger J, Bertram S, *et al.* Loss of Survivin influences liver regeneration and is associated with impaired Aurora B function. *Cell Death Differ* 2013; **20**: 834–844.
- Klionsky DJ, Abdelmohsen K, Abe A, *et al.* Guidelines for the use and interpretation of assays for monitoring autophagy. *Autophagy* 2016; **12**: 1–222.
- Fan L, Yin S, Zhang E, *et al.* Role of p62 in the regulation of cell death induction. *Apoptosis* 2018; **23**: 187–193.
- Moscat J, Diaz-Meco MT. p62: a versatile multitasker takes on cancer. *Trends Biochem Sci* 2012; **37**: 230–236.
- Duran A, Linares JF, Galvez AS, *et al.* The signaling adaptor p62 is an important NF-kappaB mediator in tumorigenesis. *Cancer Cell* 2008; **13**: 343–354.
- Yan X-Y, Zhang Y, Zhang J-J, *et al.* p62/SQSTM 1 as an oncotarget mediates cisplatin resistance through activating RIP1-NF-kappaB pathway in human ovarian cancer cells. *Cancer Sci* 2017; **108**: 1405–1413.
- Jin Z, Li Y, Pitti R, *et al.* Cullin3-based polyubiquitination and p62-dependent aggregation of caspase-8 mediate extrinsic apoptosis signaling. *Cell* 2009; **137**: 721–735.

20. Jain A, Lamark T, Sjøttem E, et al. p62/SQSTM1 is a target gene for transcription factor NRF2 and creates a positive feedback loop by inducing antioxidant response element-driven gene transcription. *J Biol Chem* 2010; **285**: 22576–22591.
21. Hewitt G, Carroll B, Sarallah R, et al. SQSTM1/p62 mediates crosstalk between autophagy and the UPS in DNA repair. *Autophagy* 2016; **12**: 1917–1930.
22. Wang Y, Zhang N, Zhang L, et al. Autophagy regulates chromatin ubiquitination in DNA damage response through elimination of SQSTM1/p62. *Mol Cell* 2016; **63**: 34–48.
23. Abdelbary EH, Ibrahim DA, Abdelgawad M. Autophagy-related molecules, light chain 3B, p62, and beclin 1, as prognostic markers in triple-negative breast cancer. *Egyptian Journal of Pathology* 2017; **37**: 8–16.
24. Li S-S, Xu L-Z, Zhou W, et al. p62/SQSTM1 interacts with vimentin to enhance breast cancer metastasis. *Carcinogenesis* 2017; **38**: 1092–1103.
25. Li Z, Li Y, Liu J, et al. Overexpression of cytoplasmic p62 protein is associated with poor prognosis in gastric adenocarcinoma. *Int J Clin Exp Pathol* 2016; **9**: 8492–8498.
26. Liu JL, Chen FF, Lung J, et al. Prognostic significance of p62/SQSTM1 subcellular localization and LC3B in oral squamous cell carcinoma. *Br J Cancer* 2014; **111**: 944–954.
27. Ruan H, Xu J, Wang L, et al. The prognostic value of p62 in solid tumor patients: a meta-analysis. *Oncotarget* 2018; **9**: 4258–4266.
28. Sample A, Zhao B, Wu C, et al. The autophagy receptor adaptor p62 is up-regulated by UVA radiation in melanocytes and in melanoma cells. *Photochem Photobiol* 2018; **94**: 432–437.
29. Schläfli AM, Adams O, Galván JA, et al. Prognostic value of the autophagy markers LC3 and p62/SQSTM1 in early-stage non-small cell lung cancer. *Oncotarget* 2016; **7**: 39544–39555.
30. Schmitz KJ, Ademi C, Bertram S, et al. Prognostic relevance of autophagy-related markers LC3, p62/sequestosome 1, Beclin-1 and ULK1 in colorectal cancer patients with respect to KRAS mutational status. *World J Surg Oncol* 2016; **14**: 189.
31. Zhu L, Wang Y, He J, et al. Cytoplasmic SQSTM1/P62 accumulation predicates a poor prognosis in patients with malignant tumor. *J Cancer* 2018; **9**: 4072–4086.
32. Bosman FT, Carneiro F, Hruban RH, et al. *WHO classification of tumours of the digestive system* (4th edn). International Agency for Research on Cancer: Lyon, 2010; 205–216.
33. Rautou P-E, Mansouri A, Lebrec D, et al. Autophagy in liver diseases. *J Hepatol* 2010; **53**: 1123–1134.
34. Levene AP, Goldin RD. Physiological hepatic nuclear vacuolation—how long does it persist? *Histopathology* 2010; **56**: 426–429.
35. Thakur P, Lamoke F, Chaffin JM, et al. Dysplastic hepatocytes develop nuclear inclusions in a mouse model of viral hepatitis. *PLoS One* 2014; **9**: e99872.
36. Dou Z, Xu C, Donahue G, et al. Autophagy mediates degradation of nuclear lamina. *Nature* 2015; **527**: 105–109.
37. Dou Z, Ivanov A, Adams PD, et al. Mammalian autophagy degrades nuclear constituents in response to tumorigenic stress. *Autophagy* 2016; **12**: 1416–1417.
38. Füllgrabe J, Klionsky DJ, Joseph B. The return of the nucleus: transcriptional and epigenetic control of autophagy. *Nat Rev Mol Cell Biol* 2014; **15**: 65–74.
39. Luo M, Zhao X, Song Y, et al. Nuclear autophagy: an evolutionarily conserved mechanism of nuclear degradation in the cytoplasm. *Autophagy* 2016; **12**: 1973–1983.
40. Shin H-JR, Kim H, Oh S, et al. AMPK–SKP2–CARM1 signalling cascade in transcriptional regulation of autophagy. *Nature* 2016; **534**: 553–557.
41. Wei X, Li X, Yan W, et al. SKP2 promotes hepatocellular carcinoma progression through nuclear AMPK-SKP2-CARM1 signalling transcriptionally regulating nutrient-deprived autophagy induction. *Cell Physiol Biochem* 2018; **47**: 2484–2497.
42. Pattingre S, Espert L, Biard-Piechaczyk M, et al. Regulation of macroautophagy by mTOR and Beclin 1 complexes. *Biochimie* 2008; **90**: 313–323.
43. Pankiv S, Lamark T, Bruun J-A, et al. Nucleocytoplasmic shuttling of p62/SQSTM1 and its role in recruitment of nuclear polyubiquitinated proteins to promyelocytic leukemia bodies. *J Biol Chem* 2010; **285**: 5941–5953.
44. Lammerding J, Fong LG, Ji JY, et al. Lamins A and C but not lamin B1 regulate nuclear mechanics. *J Biol Chem* 2006; **281**: 25768–25780.
45. Maniotis AJ, Chen CS, Ingber DE. Demonstration of mechanical connections between integrins, cytoskeletal filaments, and nucleoplasm that stabilize nuclear structure. *Proc Natl Acad Sci U S A* 1997; **94**: 849–854.
46. Bozler J, Nguyen HQ, Rogers GC, et al. Condensins exert force on chromatin-nuclear envelope tethers to mediate nucleoplasmic reticulum formation in *Drosophila melanogaster*. *G3 (Bethesda)* 2015; **5**: 341–352.
47. Rezk S, Brynes RK, Nelson V, et al. Beta-catenin expression in thyroid follicular lesions: potential role in nuclear envelope changes in papillary carcinomas. *Endocr Pathol* 2004; **15**: 329–337.

## SUPPLEMENTARY MATERIAL ONLINE

**Figure S1** 3D imaging of immunofluorescence-labelled (lamin B) isolated cell nuclei in X-, Y- and Z-axes

**Figure S2** Immunoreactivity of autophagy-related proteins (ATG)7, ATG12 and Beclin1 in nuclear inclusions of HCC

**Table S1** Immunohistochemistry antibodies and staining protocols for ubiquitin, p62, LC3B, cathepsin B and cathepsin D

**Table S2** 3D imaging of the inclusions: antibodies used for double immunofluorescence and staining conditions

**Table S3** 3D imaging of the inclusions: antibodies used for triple immunofluorescence and staining conditions

**Table S4** Immunohistochemistry antibodies and staining protocols for ATG proteins and Beclin1

**Movie S1** 3D nuclear imaging with double immunofluorescence